

# Yang monopoles and emergent three-dimensional topological defects in interacting bosons

Yangqian Yan, Qi Zhou

*Department of Physics and Astronomy, Purdue University, West Lafayette, IN, 47906*

(Dated: September 21, 2022)

Yang monopole as a zero-dimensional topological defect has been well established in multiple fields in physics. However, it remains an intriguing question to understand interaction effects on Yang monopoles. Here, we show that collective motions of many interacting bosons give rise to exotic topological defects that are distinct from Yang monopoles seen by a single particle. Whereas interactions may distribute Yang monopoles in the parameter space or glue them to a single giant one of multiple charges, three-dimensional topological defects also arise from continuous manifolds of degenerate many-body eigenstates. Their projections in lower dimensions lead to knotted nodal lines and nodal rings. Our results suggest that ultracold bosonic atoms can be used to create emergent topological defects and directly measure topological invariant that are not easy to access in solids.

Yang monopoles [1] play a crucial role in non-abelian gauge theories and have influential impacts in multiple subareas of physics. In high energy physics, they lay the foundation of Yang-Mills theory and standard model [2–6]. In condensed matter physics, Yang monopoles give rise to nontrivial topological quantum states characterized by the second Chern number,  $C_2$  [7–11]. In a 5D parameter space, a Yang monopole represents a zero-dimensional point defect with a four-fold degeneracy. Away from a Yang monopole, a spin-3/2 or pseudospin-3/2 could see such point topological defect from either local nonabelian Berry curvatures or  $C_2$ . When a 4D surface encloses a single Yang monopole,  $C_2 = 1$ . One thus can view a Yang monopole as a magnetic monopole of “charge” 1.

Whereas Yang monopoles remained a theoretical concept for decades, Sugawa, *et al.*, at NIST delivered a Yang monopole for the first time in laboratories by engineering the couplings among four hyperfine spin states of ultracold bosonic atoms [10]. Each boson in this experiment represents a pseudospin-3/2. The advantage of using bosons is that all particles populate the same place in the parameter space such that local Berry curvatures can be detected. In fact, about half of current ultracold atom experiments have used bosons to probe local Berry curvatures in a wide range of topological quantum systems [12–18]. Integrating local nonabelian Berry curvatures,  $C_2$  has been measured in the NIST experiment. Very recently,  $C_2$  has also been measured in optical lattices and photonic crystals [19, 20].

Whereas Yang monopoles have been well established in non-interacting systems, how to understand interactions on these monopoles remains an outstanding question. Since a single spin-3/2 or pseudospin-3/2 sees a monopole at the origin of the parameter space, a fundamental question naturally arises, are topological defects seen by a collection of many interacting spin-3/2s or pseudospin-3/2s the same as those seen by each individual one? In this Letter, we show that interactions

allow physicists to access completely different topological defects arising from collective motions of many particles. These emergent topological defects signify the vital importance of interactions on Yang monopoles, and demonstrate the power of ultracold bosonic atoms in creating novel topological phenomena and detecting topological invariants that are not easy in solids.

Our main results are summarized as follows. For odd particle numbers, repulsive interactions distribute Yang monopoles evenly on the quantization axis in the parameter space, and attractive interactions glue multiple Yang monopoles to a single one of “charge”  $N^2$  at the origin. In contrast, for  $N = 4n + 2$ , where  $n$  is a non-zero integer, interactions produce multiple 3D topological defects. Projecting them to lower-dimensional subspaces result in nodal lines and nodal rings. When  $N = 4n$ , the many-body ground state is unique for repulsive interactions, and no topological defect can be seen by the ground state. The results of attractive interactions are similar to those for  $N = 4n + 2$ . Here, nodal lines and nodal rings emerge purely from interaction effects in bosons, unlike those studied in non-interacting electronic systems [21–25]. We also show how to use ultracold bosons to directly measure the topological invariants in laboratories.

Our work was motivated by a recent paper by Ho and Li [11]. Based on a mean field approach, this pioneering work shows that a point singularity in the parameter space, such as a Yang monopole or a Dirac monopole, may be stretched into an extended manifold. In this mean field approach, all pseudospin-3/2s are described by the same condensate wave function. The exact solution we provide here for a generic  $N$ -body system, however, shows that the many-body ground state becomes degenerate in certain locations in the parameter space. These *degenerate many-body eigenstates* give rise to the aforementioned novel topological defects beyond mean-field predictions.

The single-particle Hamiltonian that describes a Yang

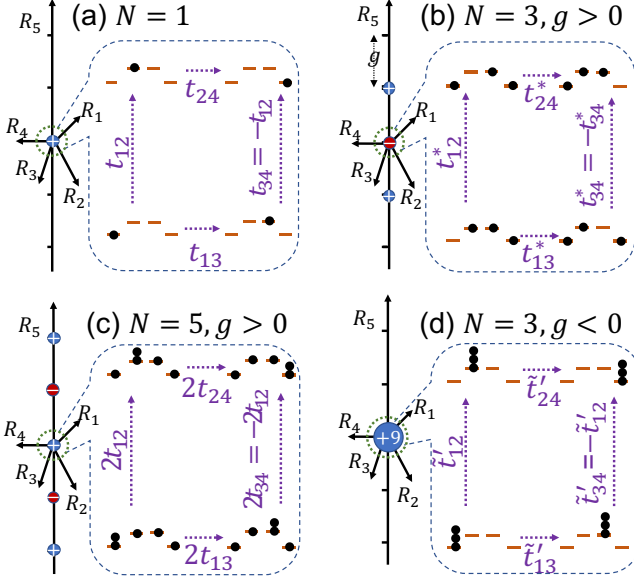


FIG. 1. (Color online) Schematic of Yang monopoles for odd number of particles. Blue (red) spheres show the positively (negatively) charged monopoles. Charges are denoted inside the sphere. (a-c),  $g > 0$ ,  $N = 1, 3, 5$ . (d)  $g < 0$ ,  $N = 3$ . Insets illustrate effective Hamiltonians near the origin. Orange solid lines and black dots represent single particle states and bosons, respectively. Dashed arrows show effective couplings.

monopole is written as [11, 25]

$$\hat{K} = -R_z \tau_z \otimes \hat{n} \cdot \vec{\sigma} - R_x \tau_x - R_y \tau_y, \quad (1)$$

where  $\vec{\sigma}$  and  $\vec{\tau}$  are two spin-1/2 operators, and  $\hat{n}$  is a unit vector. A single-mode approximation has been taken for the orbital part of the wavefunction, i.e., bosons share the same spatial wavefunction. Eq.(1) defined in a 5D parameter space,  $\mathbf{R} = (R_x, R_y, R_z n_x, R_z n_y, R_z n_z)$ , describes a spin-3/2 particle. For the convenience of later discussions, we rewrite this Hamiltonian,

$$\hat{K} = \sum_i \epsilon_i \hat{a}_i^\dagger \hat{a}_i + \sum_{i < j} t_{ij} \hat{a}_i^\dagger \hat{a}_j + h.c., \quad (2)$$

which describes four lattice sites coupled by certain inter-site tunnelings  $t_{ij}$ , as shown in Fig. 1(a).  $\epsilon_i$  is the onsite energy, and  $-\epsilon_1 = \epsilon_2 = \epsilon_3 = -\epsilon_4 = R_z n_z$ .  $t_{13} = t_{31}^* = t_{24} = t_{42}^* = -R_x + iR_y$ ,  $t_{12} = t_{21}^* = -t_{34} = -t_{43}^* = -R_z n_x + iR_z n_y$ . Other tunnelings are zero. Because the single-particle Hamiltonian is invariant under time reversal transformation and the total spin is half integer, Kramers theorem states that every eigenstate is at least doubly degenerate. For many-body systems, we consider the Hamiltonian,

$$\hat{H} = \hat{K} + \hat{U}, \quad \hat{U} = g \sum_{i=1}^4 (\hat{a}_i^\dagger a_i)^2, \quad (3)$$

where  $g$  is the onsite interaction strength. Because the interaction respects the time reversal symmetry, for even number of particles, the Kramers theorem still apply. In NIST experiments, the interactions among the four hyperfine spin states may take more complex forms. Here, Eq. (3) serves as an illuminating example to reveal fundamental interaction effects on Yang monopoles. A Yang monopole may also be realized using other schemes, such as coupled four lattice sites described by Eq.(2). It is then natural to consider  $\hat{H}$  in Eq. (3) as onsite interactions are dominant.

We solve  $\hat{H}$  exactly and obtain the many-body eigenstates  $|\Psi_m\rangle$  for  $N$  bosons.  $|\Psi_m\rangle$  is expanded using Fock states,  $|\Psi_m\rangle = \sum_{\{n_i\}} \alpha_m \{n_i\} |n_1, n_2, n_3, n_4\rangle$ , where  $n_i$  represents the occupation in the  $i$ th lattice site and  $\sum_{i=1}^4 n_i = N$  is satisfied. Using  $|\Psi_m\rangle$ , nonabelian Berry connections  $A_\nu^{mn} = -i \langle \Psi_m | \partial_\nu | \Psi_n \rangle$  and nonabelian Berry curvatures  $F_{\mu\nu}^{mn} = \partial_\mu A_\nu^{mn} - \partial_\nu A_\mu^{mn} + i[A_\mu, A_\nu]^{mn}$  are obtained. Whereas all bosons occupy the same place in the parameter space, their collective motions lead to much richer topological defects than those seen by a single bosons, or equivalently, a single pseudospin-3/2. When a nodal point is observed, we compute  $C_2$  using [5, 6]

$$C_2 = \frac{1}{32\pi^2} \int_{S^4} d\mathbf{R} \epsilon_{\mu\nu\rho\lambda} (\text{Tr}[F_{\mu\nu} F_{\rho\lambda}] - \text{Tr}[F_{\mu\nu}] \text{Tr}[F_{\rho\lambda}]), \quad (4)$$

where  $\epsilon_{\mu\nu\rho\lambda}$  is Levi-Civita symbol. When nodal lines or nodal rings are observed,  $Z_2$  invariants are computed, which will be discussed later.

Away from the origin of the parameter space, the single-particle ground state becomes two-fold degenerate. Thus, for  $N$  noninteracting bosons, there are  $N + 1$  degenerate many-body eigenstates. Both the nonabelian Berry connections, which form a  $(N + 1) \times (N + 1)$  matrix, and nonabelian Berry curvatures can be calculated analytically, and  $C_2$  reads [26]

$$C_2^o = N(N + 1)(N + 2)/6, \quad (5)$$

where the superscript  $o$  denotes the results for non-interacting bosons.

Turning on interactions, results become completely different. Whereas the exact values of  $A_\nu^{mn}$  and  $F_{\mu\nu}^{mn}$  require numerical calculations, topological defects that determine the global topological properties of the parameter space are analytically studied. We start from odd  $N$ . When  $g > 0$ , there are  $N$  points on the  $R_5 = R_z n_z$  axis, where the many-body ground state becomes four-fold degenerate. The origin is a simple one, since  $\hat{K} = 0$ , and there are four different ways to distribute  $N \in \text{odd}$  bosons in four equivalent lattice sites to minimize the interaction energy, as shown in Fig. 1(b) and (c). Away from the origin, four-fold degenerate points also exist on the  $R_5$  axis. All tunnelings in Eq. (2) vanish on this axis, as  $R_i = 0$  for  $i = 1, 2, 3$ , and 4. Many-body eigenstates are simply Fock states. The energy mismatch between different sites

$\epsilon_1 - \epsilon_2 = \epsilon_4 - \epsilon_3$  could exactly compensate the penalty of interaction energy for moving one boson from one lattice site to another. We show the simplest example for  $N = 3$ . When  $R_5 = g$ , it is straightforward to verify that the four Fock states  $|1, 1, 0, 1\rangle$ ,  $|1, 0, 1, 1\rangle$ ,  $|2, 0, 0, 1\rangle$ , and  $|1, 0, 0, 2\rangle$  become degenerate. It is also easy to verify that, for any  $N$ , the separation between two nearest points is given by  $\Delta R_5 = g$ , and the last point is located at  $R_5^* = \pm(N-1)g/2$  [shown in Fig. 1(b) and (c)].

Away from these four-fold degenerate points, the energies of the four Fock states become different, and tunnelings become finite. In the vicinity of each degenerate point, we construct an effective model using the four nearly degenerate states as the basis. Such effective model turns out to have exactly the same formula as the single-particle Hamiltonian in Eq. (2). The only difference is that the parameters,  $\epsilon_i$  and  $t_{ij}$ , are replaced by effective ones determined by both single-particle Hamiltonian and interactions. As an example, we show the effective Hamiltonian near the origin, in which the parameters are written explicitly as

$$\tilde{\epsilon}_i = (-1)^{(N-1)/2} \epsilon_i \quad (6)$$

$$\tilde{t}_{ij} = \begin{cases} t_{ij}(N+3)/4 & \text{for } N=1, 5, 9, \dots \\ t_{ij}^*(N+1)/4 & \text{for } N=3, 7, 11, \dots \end{cases} \quad (7)$$

From this observation, we conclude that each four-fold degenerate point corresponds to a Yang monopole. Using the exact results of the full Hamiltonian, we have verified numerically that  $C_2$  on any closed surface including only one of these Yang monopoles is exactly 1 or  $-1$ . It is noted that  $C_2$  of the ground state manifold, which contains two degenerate states, is much smaller than that of non-interacting systems. An infinitesimal interaction actually lifts the  $N+1$  fold degeneracy of noninteracting systems. Therefore,  $C_2$  of the ground state manifold reduces. Nevertheless, we have verified that, the total  $C_2$  of the lowest  $N+1$  bands is indeed the same as  $C_2^0$ .

A subtle difference between  $N = 1, 5, 9, \dots$  and  $N = 3, 7, 11, \dots$  exists. As shown in Fig. 1(b) and (c), it is a particle and a hole that tunnelings in the effective Hamiltonian for these two cases, respectively. Thus, the ‘‘charge’’ of the Yang monopole at the origin for  $N = 1, 5, 9, \dots$  is 1 and that for  $N = 3, 7, 11, \dots$  is  $-1$ . Similarly, for a fixed  $N$ , with increasing the distance to the origin, the ‘‘charge’’ of monopoles also alternate [26]. When the closed surface is large enough,  $C_2$  becomes 1 for all odd  $N$ .

For attractive interactions, only one monopole exists in the parameter space, and its ‘‘charge’’ is  $N^2$ . At the origin,  $|N, 0, 0, 0\rangle$ ,  $|0, N, 0, 0\rangle$ ,  $|0, 0, N, 0\rangle$ ,  $|0, 0, 0, N\rangle$  are the four degenerate many-body ground states, as all bosons prefer to occupy the same lattice site to minimize the interaction energy. Away from the origin, an effective model, which has the same formula as Eq. (2), can be constructed. Since a single-particle tunneling  $t_{ij}$  moves

one boson from one lattice site to another, it requires  $N$  steps of single-particle tunneling to coupling any of these four states. The parameters in the effective Hamiltonian are given by,

$$\tilde{\epsilon}'_i = N\epsilon_i \text{ and } \tilde{t}'_{ij} = c_N t_{ij}^N / g^{N-1}, \quad (8)$$

where  $c_N$  is a function of  $N$  [26]. Using this effective model, we obtain that the ‘‘charge’’ of the monopole is  $N^2$ . The superposition of the four Fock states actually forms a Schrodinger cat state [27–30]. Though it is not stable in the large  $N$  limit, in a few-body system [31, 32], a small cat could exist in laboratories such that a Yang monopole of ‘‘charge’’  $N^2$  is observable. For both positive and negative interactions, the second Chern number on any closed 4D surface is equal to the total charge of monopoles inside the surface [26].

We now turn to even  $N$ . If the average particle number per site is an integer, i.e.,  $N = 4n$ , where  $n$  is a finite integer, the many-body ground state becomes unique for repulsive interactions. This is best understood in the strongly interacting regime, as bosons prefer to distribute evenly in the four lattice sites so as to minimize the interaction energy. Thus, the unique ground state cannot see any topological defects. When  $g$  is negative, the many-body ground state is four-fold degenerate at the origin of the parameter space, similar to the case of odd particles. Away from the origin, an effective Hamiltonian can also be constructed in the same manner. However, the resultant effective Hamiltonian is distinct. The reason is that, the effective coupling between the Fock states, such as  $|N, 0, 0, 0\rangle$  and  $|0, N, 0, 0\rangle$ , now requires an even number steps of single-particle tunnelings. In the single-particle Hamiltonian as shown in Eq. (2),  $t_{12}$  and  $t_{34}$  differ by a minus sign. This can also be seen from Eq. (1) that  $\tau_z = \pm 1/2$  leads to a different sign of the term  $\hat{n} \cdot \vec{\sigma}$ . This minus sign remains unchanged in the effective model for odd particle numbers, as both the two effective couplings,  $\tilde{t}'_{12}$  and  $\tilde{t}'_{34}$ , are proportional to the odd powers of  $t_{12}$  and  $t_{34}$ .

For even particle numbers, the minus sign disappears. Completely different topological defects arise. We write the effective Hamiltonian as

$$\hat{H}_{\text{eff}} = a\tilde{\tau}_z \otimes \tilde{\sigma}_z + b\tilde{\tau}_x \otimes I + c\tilde{\tau}_y \otimes I + dI \otimes \tilde{\sigma}_x + eI \otimes \tilde{\sigma}_y, \quad (9)$$

where  $a = -2R_5$ ,  $b = -(R_1^2 - R_2^2)/g$ ,  $c = -2R_1 R_2/g$ ,  $d = -(R_3^2 - R_4^2)/g$ , and  $e = -2R_3 R_4/g$  for  $N = 2$ .  $\vec{\sigma}$  and  $\vec{\tau}$  are two spin-1/2s. The eigenstates of  $\tilde{\tau}_z \otimes \tilde{\sigma}_z$ ,  $|\uparrow\uparrow\rangle$ ,  $|\uparrow\downarrow\rangle$ ,  $|\downarrow\uparrow\rangle$ ,  $|\downarrow\downarrow\rangle$  correspond to  $|N, 0, 0, 0\rangle$ ,  $|0, N, 0, 0\rangle$ ,  $|0, 0, N, 0\rangle$ ,  $|0, 0, 0, N\rangle$ . The eigenenergy of  $\hat{H}_{\text{eff}}$  is written as

$$E = \pm \sqrt{a^2 + (\sqrt{b^2 + c^2} \pm \sqrt{d^2 + e^2})^2}, \quad (10)$$

which shows that eigenenergies become degenerate in certain 3D continuous manifolds.

$\{\mathcal{M}_1: b = c = 0 (R_1 = R_2 = 0)\}$  and  $\{\mathcal{M}'_1: d = e = 0 (R_3 = R_4 = 0)\}$ , both the ground and excited states are doubly degenerate.

$\{\mathcal{M}_2: a = 0, b^2 + c^2 = d^2 + e^2 (R_5 = 0, R_1^2 + R_2^2 = R_3^2 + R_4^2)\}$ , the second and the third states are degenerate, and the ground state (the fourth state) is unique.

As Kramers theorem does not apply to even number of spin-3/2s, the even-fold degeneracy is not guaranteed and  $\mathcal{M}_2$  is possible here. These three manifolds intersect at the origin in the 5D parameter space. Away from them, there is no degeneracy.  $\mathcal{M}_2$  signifies the vanishing gap between the lowest and the highest two states on any closed 4D surface. Thus,  $C_2$  is no longer an appropriate number to characterize the topological defects. Each manifold by itself is characterized by  $Z_2$  invariants. Meanwhile, the projections of them in lower dimensional lead to knotted nodal lines and nodal rings.

Since  $\mathcal{M}_1$  and  $\mathcal{M}_2$  are 3D defects in a 5D parameter space, a 1D loop can be defined without intersecting them. We note that  $\hat{H}_{\text{eff}}$  can be rewritten as a real Hamiltonian by a simple transformation,  $\tilde{\tau}_y \leftrightarrow \tilde{\tau}_z, \tilde{\sigma}_y \leftrightarrow -\tilde{\sigma}_z$ . Thus,  $\hat{H}_{\text{eff}}$  on this loop can be classified by the Berry phase [24, 33, 34],

$$\gamma_m = -i \oint_M d\mathbf{R} \cdot \langle \Psi_m | \nabla_{\mathbf{R}} | \Psi_m \rangle. \quad (11)$$

Without loss of generality, we have considered all eigenstates  $|\Psi_m\rangle$  with  $m = 1, 2, 3, 4$ . Any loop that does not interlock the defects can shrink to a single point without closing the gap,  $\gamma_m = 0$ . For a loop interlocking the defects, whether  $\gamma_1 + \gamma_2 = 0$  or  $\pi$  (or their multiples), defines a  $Z_2$  index  $\zeta_1$  for the defects [24]. For  $\mathcal{M}_1$  and  $\mathcal{M}'_1$ , we find that  $\gamma = N\pi$  for all eigenstates and  $\zeta_1 = 0$ . For  $\mathcal{M}_2$ , we find that  $\gamma = (0, \pi, \pi, 0)$  for each eigenstate and  $\zeta_1 = 1$ .

To better visualize this  $Z_2$  invariant, we project  $\mathcal{M}_1, \mathcal{M}'_1$  and  $\mathcal{M}_2$  to lower dimensions, i.e., reducing the dimension by fixing the values of certain parameters. We define  $\vec{m} = (d, e)$  and  $|\vec{m}| = \sqrt{d^2 + e^2} = (R_3^2 + R_4^2)/|g|$ , the eigenenergies in Eq. (10) reads  $E = \pm \sqrt{a^2 + (\sqrt{b^2 + c^2} \pm |\vec{m}|)^2}$ . Interestingly, this energy spectrum is identical to the one used to study nodal rings in electronic systems [24]. As shown in Fig. 2, for any finite  $|\vec{m}|$ ,  $\mathcal{M}_1$  becomes an infinite nodal line, and  $\mathcal{M}_2$  becomes a nodal ring with radius  $|\vec{m}|$ .  $\mathcal{M}'_1$  does not show up in this subspace. The dashed circles that interlock the nodal ring or the nodal line allow one to compute  $\gamma$ . Decreasing  $|\vec{m}|$ , the nodal ring shrinks and the nodal line remains unchanged. When  $|\vec{m}| = 0$ , the nodal ring reduces to a single point at the origin, and the gap does not open. In particular, this whole 3D subspace precisely becomes  $\mathcal{M}'_1$  and the eigenenergies are two-fold degenerate everywhere. For this particular set of parameters,  $\hat{H}_{\text{eff}}$  describes a quantum spin Hall effect, as  $\sigma_z = \pm 1$  corresponds to two opposite effective magnetic fields acting on

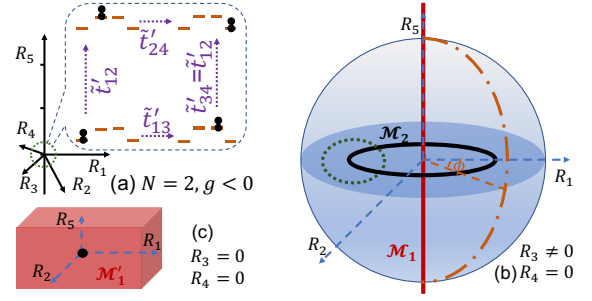


FIG. 2. (Color online) (a) The effective Hamiltonian for two particles with attractive interaction. (b-c) shows the projections of the defects in a 3D subspace with fixed  $R_3$  and  $R_4$ . (b) The red line (black ring) shows the projection of  $\mathcal{M}_1$  ( $\mathcal{M}_2$ ). The green dashed circle is a 1D loop used to calculate the  $Z_2$  index  $\zeta_1$ . The blue 2D sphere is used to calculate the  $Z_2$  index  $\zeta_2$ . The dash-dotted longitude connecting the north and south poles is used to compute  $\phi$ -dependent Wilson lines. (c)  $\mathcal{M}_2$  reduces to a point at the origin.  $\mathcal{M}'_1$  occupying the entire 3D subspace is shown as a red box.

$\vec{\tau}$ . When  $\vec{m}$  changes sign, the nodal ring and nodal line appear again, which signifies the stability of the nodal ring.

The nodal ring is also characterized by another  $Z_2$  index,  $\zeta_2 = 0, 1$  [24, 33]. On any 2D sphere that does not touch  $\mathcal{M}_2$ , the lowest two eigenstates are separated from the highest two. The lowest two states intersect at the north and south poles. Any longitude connecting the north pole and the south pole defines a Wilson line [35],  $W_{ij}(\phi) = \langle \Psi_i(\pi, \phi) | \hat{W} | \Psi_j(0, \phi) \rangle$ , where  $|\Psi_{i=1,2}(0, \phi)\rangle$  and  $|\Psi_{i=1,2}(\pi, \phi)\rangle$  are the lowest two eigenstate states at the north and south poles, respectively,  $\phi \in [0, 2\pi)$  is the azimuthal angle, and  $\hat{W} = \prod_{k=1}^N \hat{P}_k$ ,  $\hat{P}_k \sum_{i=1}^2 |\Psi_i(\theta_k, \phi)\rangle \langle \Psi_i(\theta_k, \phi)|$  is the projection operator in the  $k$ th step if we divide the longitude to  $\mathcal{N}$  steps. Physically,  $W_{ij}(\phi)$  characterizes the probability of occupying either eigenstate at the south pole if the initial state is an arbitrary superposition of the eigenstate at the north pole after an adiabatic evolution along the longitude. As  $\hat{H}_{\text{eff}}$  can be rewritten as a real Hamiltonian,  $W_{ij}(\phi)$  can be expressed as an orthogonal matrix after an appropriate unitary transformation. Thus,  $\xi(\phi) = W_{11}(\pi/2, \phi) + iW_{12}(\pi/2, \phi)$  defines a winding number and the  $Z_2$  index  $\zeta_2$  through

$$\zeta_2 = \text{mod}(n_w, 2), \quad n_w = -\frac{i}{2\pi} \int_0^{2\pi} \xi^*(\phi) \partial_\phi \xi(\phi). \quad (12)$$

For our effective model  $\hat{H}_{\text{eff}}$ , we find that  $\zeta_2 = 1$  for any 2D sphere that includes the nodal ring. Otherwise,  $\zeta_2 = 0$ . Thus, the nodal ring defines a topological phase transition where  $\zeta_2$  changes its value. For repulsive interactions,  $\mathcal{M}_1$  and  $\mathcal{M}'_1$  switch with  $\mathcal{M}_2$  [26]. Whereas we have been focusing on each individual degenerate manifolds, a finite linking number exists [26]. While the

topological defects are derived in the strongly interacting regime, we numerically verified that they hold even for weakly interacting systems.

It is worth mentioning that, with increasing  $N$ , the energy splitting between different eigenstates decreases. Thus, to better resolve these topological defects and the associated topological invariants, experimentalists could increase interaction strength, or use a mesoscopic system or a few-body system [31, 32].

Whereas our theoretical results are general, it is useful to discuss the parameter regimes explored by the current NIST experiment, where condensates in big traps are prepared. Due to the small scattering length  $a_s$  and the extended orbital wavefunction, interaction strength is very weak. For instance, for  $a_s = 5\text{nm}$ ,  $N = 10^5$ , trapping frequency  $\omega = 2\pi * 70\text{Hz}$ , interaction strength  $g \approx 0.04\text{Hz}$ , which is too weak to have significant effects in current experiments. The main experimental results are well explained by non-interacting pictures. When interaction becomes large, much richer topological defects discussed in this Letter emerge. To increase  $g$ , either the scattering length or the confinement can be increased, for instance, using few-body systems in tight confining traps [31, 32]. Furthermore, an alternative approach of realizing the model in Eq. (3) and Eq. (9) is to use lattice directly in the real space. For instance, using optical lattices [36, 37], the tunneling between the four lattice sites in each isolated plaque can be designed so as to deliver the Hamiltonian in Eq. (1). The effective Hamiltonians in Eq. (9) could then be explored by turning on strong interactions, or directly engineering the inter-site couplings in the single-particle level.

A unique advantage of ultracold atoms is that topological defects and the associated topological invariants can be directly probed. To measure the first  $Z_2$  invariant,  $\zeta_1$ , the local Berry curvature could be measured to extract the Berry phase accumulated in a 1D loop [10, 14, 38–42]. To measure the second  $Z_2$  invariant,  $\zeta_2$ ,  $W_{ij}(\phi)$  for each  $\phi$  can be measured in the same manner as the reconstruction of Wilson line in a recent experiment [43]. Controllable perturbations can also be introduced in cold atom experiments by manipulating microscopic parameters. For small perturbations, our main results remain unchanged. For large perturbations, new effective Hamiltonians and new classes of topological defect may arise. We hope that our work will stimulate more studies on using ultracold atoms to create and measure topological defects in high dimensions, in particular, those emerged from interactions.

QZ acknowledges useful discussions with T.L. Ho, I. Spielman, and S. Sugawa. YY acknowledges useful discussions with C. Li. This work is supported by startup funds from Purdue University.

- 
- [1] C. N. Yang and R. L. Mills, “Conservation of Isotopic Spin and Isotopic Gauge Invariance,” *Phys. Rev.* **96**, 191 (1954).
  - [2] C. N. Yang, “Generalization of Diracs monopole to  $SU_2$  gauge fields,” *J. Math. Phys.* **19**, 320 (1978).
  - [3] G. ’t Hooft, “The standard model of particle physics,” *Nature (London)* **448**, 270 (2007).
  - [4] G. ’t Hooft, “Magnetic monopoles in unified gauge theories,” *Nucl. Phys. B* **79**, 276 (1974).
  - [5] S.-S. Chern, “Characteristic Classes of Hermitian Manifolds,” *Ann. Math.* **47**, 85 (1946).
  - [6] S. Chern, *Topics in differential geometry* (The Institute for Advanced Study, Princeton, 1951).
  - [7] C.-H. Chern, H.-D. Chen, C. Wu, J.-P. Hu, and S.-C. Zhang, “Non-Abelian Berry phase and Chern numbers in higher spin-pairing condensates,” *Phys. Rev. B* **69**, 214512 (2004).
  - [8] D. Xiao, J. Shi, D. P. Clougherty, and Q. Niu, “Theory of electric polarization induced by inhomogeneity in crystals,” ArXiv e-prints (2007), [arXiv:0711.1855](https://arxiv.org/abs/0711.1855).
  - [9] X.-L. Qi, T. L. Hughes, and S.-C. Zhang, “Topological field theory of time-reversal invariant insulators,” *Phys. Rev. B* **78**, 195424 (2008).
  - [10] S. Sugawa, F. Salces-Carcoba, A. R. Perry, Y. Yue, and I. B. Spielman, “Observation of a non-Abelian Yang Monopole: From New Chern Numbers to a Topological Transition,” [arXiv:1610.06228](https://arxiv.org/abs/1610.06228).
  - [11] T.-L. Ho and C. Li, “The Chern Numbers of Interaction-stretched Monopoles in Spinor Bose Condensates,” [arXiv:1704.03833](https://arxiv.org/abs/1704.03833).
  - [12] M. Aidelsburger, M. Atala, M. Lohse, J. T. Barreiro, B. Paredes, and I. Bloch, “Realization of the hofstadter hamiltonian with ultracold atoms in optical lattices,” *Phys. Rev. Lett.* **111**, 185301 (2013).
  - [13] H. Miyake, G. A. Siviloglou, C. J. Kennedy, W. C. Burton, and W. Ketterle, “Realizing the Harper Hamiltonian with Laser-Assisted Tunneling in Optical Lattices,” *Phys. Rev. Lett.* **111**, 185302 (2013).
  - [14] M. Atala, M. Aidelsburger, J. T. Barreiro, D. Abanin, T. Kitagawa, E. Demler, and I. Bloch, “Direct measurement of the Zak phase in topological Bloch bands,” *Nat. Phys.* **9**, 795 (2013).
  - [15] M. D. Schroer, M. H. Kolodrubetz, W. F. Kindel, M. Sandberg, J. Gao, M. R. Vissers, D. P. Pappas, A. Polkovnikov, and K. W. Lehnert, “Measuring a Topological Transition in an Artificial Spin-1/2 System,” *Phys. Rev. Lett.* **113**, 050402 (2014).
  - [16] M. W. Ray, E. Ruokokoski, S. Kandel, M. Möttönen, and D. S. Hall, “Observation of Dirac monopoles in a synthetic magnetic field,” *Nature (London)* **505**, 657 (2014).
  - [17] M. Aidelsburger, M. Lohse, C. Schweizer, M. Atala, J. T. Barreiro, S. Nascimbène, N. R. Cooper, I. Bloch, and N. Goldman, “Measuring the Chern number of Hofstadter bands with ultracold bosonic atoms,” *Nat. Phys.* **11**, 162 (2015).
  - [18] M. Lohse, C. Schweizer, O. Zilberberg, M. Aidelsburger, and I. Bloch, “A Thouless quantum pump with ultracold bosonic atoms in an optical superlattice,” *Nat. Phys.* **12**, 350 (2016).
  - [19] M. Lohse, C. Schweizer, H. M. Price, O. Zilberberg, and I. Bloch, “Exploring 4D Quantum Hall Physics with a

- 2D Topological Charge Pump,” [arXiv:1705.08371](https://arxiv.org/abs/1705.08371).
- [20] O. Zilberberg, S. Huang, J. Guglielmon, M. Wang, K. Chen, Y. E. Kraus, and M. C. Rechtsman, “Photonic topological pumping through the edges of a dynamical four-dimensional quantum Hall system,” [arXiv:1705.08361](https://arxiv.org/abs/1705.08361).
- [21] A. A. Burkov, M. D. Hook, and L. Balents, “Topological nodal semimetals,” *Phys. Rev. B* **84**, 235126 (2011).
- [22] A. P. Schnyder, P. M. R. Brydon, and C. Timm, “Types of topological surface states in nodal noncentrosymmetric superconductors,” *Phys. Rev. B* **85**, 024522 (2012).
- [23] P. Hosur, X. Dai, Z. Fang, and X.-L. Qi, “Time-reversal-invariant topological superconductivity in doped Weyl semimetals,” *Phys. Rev. B* **90**, 045130 (2014).
- [24] C. Fang, Y. Chen, H.-Y. Kee, and L. Fu, “Topological nodal line semimetals with and without spin-orbital coupling,” *Phys. Rev. B* **92**, 081201 (2015).
- [25] B. Lian and S.-C. Zhang, “Five-dimensional generalization of the topological Weyl semimetal,” *Phys. Rev. B* **94**, 041105 (2016).
- [26] The supplemental materials at TO-BE-INSERT-BY-THE-EDITOR contains calculation of non-interacting  $C_2$ ; location and “charge” of the Yang monopole for odd  $N$  and positive  $g$ ;  $C_2$  for odd  $N$ ; expression for  $c_N$ ; 3D topological defects for even number of particles with repulsive interaction; linking number.
- [27] W. H. Zurek, “Decoherence and the transition from quantum to classical,” *Phys. Today* **44**, 36 (1991).
- [28] C. Monroe, D. M. Meekhof, B. E. King, and D. J. Wineland, “A “Schrodinger Cat” Superposition State of an Atom,” *Science* **272**, 1131 (1996).
- [29] T.-L. Ho and C. V. Ciobanu, “The Schrödinger Cat Family in Attractive Bose Gases,” *J. Low Temp. Phys.* **135**, 257 (2004).
- [30] E. J. Mueller, T.-L. Ho, M. Ueda, and G. Baym, “Fragmentation of Bose-Einstein condensates,” *Phys. Rev. A* **74**, 033612 (2006).
- [31] A. N. Wenz, G. Zürn, S. Murmann, I. Brouzos, T. Lompe, and S. Jochim, “From Few to Many: Observing the Formation of a Fermi Sea One Atom at a Time,” *Science* **342**, 457 (2013).
- [32] G. Zürn, A. N. Wenz, S. Murmann, A. Bergschneider, T. Lompe, and S. Jochim, “Pairing in Few-Fermion Systems with Attractive Interactions,” *Phys. Rev. Lett.* **111**, 175302 (2013).
- [33] A. Hatcher, *Algebraic Topology* (Cambridge University Press, Cambridge, UK, 2002).
- [34] Chen Fang and Hongming Weng and Xi Dai and Zhong Fang, “Topological nodal line semimetals,” *Chin. Phys. B* **25**, 117106 (2016).
- [35] R. Yu, X. L. Qi, A. Bernevig, Z. Fang, and X. Dai, “Equivalent expression of  $Z_2$  topological invariant for band insulators using the non-Abelian Berry connection,” *Phys. Rev. B* **84**, 075119 (2011).
- [36] S. Nascimbène, Y.-A. Chen, M. Atala, M. Aidelsburger, S. Trotzky, B. Paredes, and I. Bloch, “Experimental Realization of Plaquette Resonating Valence-Bond States with Ultracold Atoms in Optical Superlattices,” *Phys. Rev. Lett.* **108**, 205301 (2012).
- [37] H.-N. Dai, B. Yang, A. Reingruber, H. Sun, X.-F. Xu, Y.-A. Chen, Z.-S. Yuan, and J.-W. Pan, “Observation of Four-body Ring-exchange Interactions and Anyonic Fractional Statistics,” [arXiv:1602.05709](https://arxiv.org/abs/1602.05709).
- [38] V. Gritsev and A. Polkovnikov, “Dynamical quantum hall effect in the parameter space,” *Proc. Natl. Acad. Sci.* **109**, 6457 (2012).
- [39] H. M. Price and N. R. Cooper, “Mapping the Berry curvature from semiclassical dynamics in optical lattices,” *Phys. Rev. A* **85**, 033620 (2012).
- [40] P. Hauke, M. Lewenstein, and A. Eckardt, “Tomography of Band Insulators from Quench Dynamics,” *Phys. Rev. Lett.* **113**, 045303 (2014).
- [41] L. Duca, T. Li, M. Reitter, I. Bloch, M. Schleier-Smith, and U. Schneider, “An Aharonov-Bohm interferometer for determining Bloch band topology,” *Science* **347**, 288.
- [42] M. Kolodrubetz, “Measuring the Second Chern Number from Nonadiabatic Effects,” *Phys. Rev. Lett.* **117**, 015301 (2016).
- [43] T. Li, L. Duca, M. Reitter, F. Grusdt, E. Demler, M. Endres, M. Schleier-Smith, I. Bloch, and U. Schneider, “Bloch state tomography using Wilson lines,” *Science* **352**, 1094 (2016).

# Supplemental Material of “Yang monopoles and emergent three-dimensional topological defects in interacting bosons”

Yangqian Yan, Qi Zhou

Department of Physics and Astronomy, Purdue University, West Lafayette, IN, 47906

(Dated: September 21, 2022)

## NON-INTERACTING $C_2$

Single-particle ground state of the Hamiltonian in Eq. (1) of the main text is doubly degenerate. Denote the two states as  $\psi_a$  and  $\psi_b$ , and define  $A_{\mu\nu}^{mn} = -i \langle \partial_\mu \psi_m | \partial_\nu \psi_n \rangle$ , the Berry curvature reads

$$F_{\mu\nu}^{mn} = A_{\mu\nu}^{mn} - A_{\nu\mu}^{mn} + i[A_\mu, A_\nu]. \quad (\text{S1})$$

Because of the time-reversal symmetry, the traces of the Berry connection and the Berry curvature are zero,

$$A_\mu^{aa} = -A_\mu^{bb}, \quad \text{Tr} F_{\mu\nu} = 0. \quad (\text{S2})$$

We also have  $A_{\mu\nu}^{aa} = A_{\nu\mu}^{bb}$ . Defining

$$\tilde{A}_{\mu\nu} = \begin{pmatrix} A_{\mu\nu}^{aa} & A_{\mu\nu}^{ab} \\ A_{\mu\nu}^{ba} & -A_{\mu\nu}^{aa} \end{pmatrix} \quad (\text{S3})$$

$$\tilde{F}_{\mu\nu} = \tilde{A}_{\mu\nu} + iA_\mu A_\nu, \quad (\text{S4})$$

and using the property of the Levi-Civita symbol, we express the second Chern number using an alternative form,

$$C_2^a(1) = \frac{1}{32\pi^2} \int_{S^4} d\mathbf{R} \epsilon_{\mu\nu\rho\lambda} \text{Tr}[F_{\mu\nu} F_{\rho\lambda}] = \frac{1}{8\pi^2} \int_{S^4} d\mathbf{R} \epsilon_{\mu\nu\rho\lambda} \text{Tr}[\tilde{F}_{\mu\nu} \tilde{F}_{\rho\lambda}]. \quad (\text{S5})$$

The above results can be generalized to  $N$  particles.

For  $N$  non-interacting bosons, there are  $N + 1$  degenerate ground states. Using Fock states as basis states, the ground state reads  $|N - i, i\rangle$ , where  $i$  takes the values of  $0, 1, 2, \dots, N$ ; here  $|N - i, i\rangle$  represent the  $N - i$  bosons in state  $\psi_a$  and  $i$  bosons in state  $\psi_b$ . The Berry connection  $A_\mu$  and matrix  $A_{\mu\nu}$  are tridiagonal in the Fock state basis.

$$A_\mu^{i-1,i} = -i \langle N - i + 1, i - 1 | \partial_\mu | N - i, i \rangle = \sqrt{i(N - 1 + 1)} A_\mu^{ab} \quad (\text{S6})$$

$$A_\mu^{i,i-1} = -i \langle N - i, i | \partial_\mu | N - i + 1, i - 1 \rangle = \sqrt{i(N - 1 + 1)} A_\mu^{ba} \quad (\text{S7})$$

$$A_\mu^{i,i} = -i \langle N - i, i | \partial_\mu | N - i, i \rangle = (N - i) A_\mu^{aa} + i A_\mu^{bb} = (N - 2i) A_\mu^{aa}. \quad (\text{S8})$$

The same holds for the  $\tilde{A}_{\mu\nu}$  matrix,

$$\tilde{A}_{\mu\nu}^{i-1,i} = -i \langle N - i + 1, i - 1 | \overleftrightarrow{\partial_\mu \partial_\nu} | N - i, i \rangle = \sqrt{i(N - 1 + 1)} A_{\mu\nu}^{ab} \quad (\text{S9})$$

$$\tilde{A}_{\mu\nu}^{i,i-1} = -i \langle N - i, i | \overleftrightarrow{\partial_\mu \partial_\nu} | N - i + 1, i - 1 \rangle = \sqrt{i(N - 1 + 1)} A_{\mu\nu}^{ba} \quad (\text{S10})$$

$$\tilde{A}_{\mu\nu}^{i,i} = (N - 2i) A_{\mu\nu}^{aa}. \quad (\text{S11})$$

Note that  $A_\mu^{xy}$  and  $A_{\mu\nu}^{xy}$  are for single particle if  $x, y$  is  $a$  or  $b$  and are for  $N$  particles otherwise. Same as that for  $N = 1$ , the second Chern number for arbitrary  $N$  can also be calculated using Eq. (S5).

We break the integrand  $\epsilon_{\mu\nu\rho\lambda} \text{Tr}[\tilde{F}_{\mu\nu} \tilde{F}_{\rho\lambda}]$  into two parts,  $\epsilon_{\mu\nu\rho\lambda} \text{Tr}[\tilde{F}_{\mu\nu} \tilde{A}_{\rho\lambda}]$  and  $2i \epsilon_{\mu\nu\rho\lambda} \text{Tr}[\tilde{A}_{\mu\nu} A_\rho A_\lambda]$  (note that  $\epsilon_{\mu\nu\rho\lambda} \text{Tr}[A_\mu A_\nu A_\rho A_\lambda]$  is 0). Writing down the trace explicitly and expressing the two terms in terms of the single particle quantities, we obtain

$$\text{Tr}[\tilde{A}_{\mu\nu} \tilde{A}_{\rho\lambda}] = \sum_i \tilde{A}_{\mu\nu}^{ii} \tilde{A}_{\rho\lambda}^{ii} + \sum_i \tilde{A}_{\mu\nu}^{i,i+1} \tilde{A}_{\rho\lambda}^{i+1,i} + \sum_i \tilde{A}_{\mu\nu}^{i,i-1} \tilde{A}_{\rho\lambda}^{i-1,i} \quad (\text{S12})$$

$$= \sum_{i=0}^N (N - 2i)^2 \tilde{A}_{\mu\nu}^{aa} \tilde{A}_{\rho\lambda}^{aa} + \sum_{i=0}^{N-1} (i + 1)(N - i) \left( \tilde{A}_{\mu\nu}^{ab} \tilde{A}_{\rho\lambda}^{ba} + \tilde{A}_{\mu\nu}^{ba} \tilde{A}_{\rho\lambda}^{ab} \right) \quad (\text{S13})$$

$$\text{Tr}[\tilde{A}_{\mu\nu} A_\rho A_\lambda] = \sum_i \tilde{A}_{\mu\nu}^{ii} \left( A_\rho^{i,i+1} A_\lambda^{i+1,i} + A_\rho^{i,i-1} A_\lambda^{i-1,i} \right) \quad (\text{S14})$$

$$+ \sum_i \tilde{A}_{\mu\nu}^{i,i-1} \left( A_\rho^{i-1,i-1} A_\lambda^{i-1,i} + A_\rho^{i-1,i} A_\lambda^{i,i} \right) \quad (\text{S15})$$

$$+ \sum_i \tilde{A}_{\mu\nu}^{i,i+1} \left( A_\rho^{i+1,i+1} A_\lambda^{i+1,i} + A_\rho^{i+1,i} A_\lambda^{i,i} \right) \quad (\text{S16})$$

$$= \sum_{i=0}^N (N-2i)(N-i)(i+1) \left( A_{\mu\nu}^{aa} A_\rho^{ab} A_\lambda^{ba} + A_{\mu\nu}^{ba} A_\rho^{aa} A_\lambda^{ab} + A_{\mu\nu}^{ab} A_\rho^{ba} A_\lambda^{aa} \right) \quad (\text{S17})$$

$$+ \sum_{i=0}^N (N-2i)(N-i+1)i \left( A_{\mu\nu}^{aa} A_\rho^{ba} A_\lambda^{ab} + A_{\mu\nu}^{ba} A_\rho^{ab} A_\lambda^{aa} + A_{\mu\nu}^{ab} A_\rho^{aa} A_\lambda^{ba} \right) \quad (\text{S18})$$

Using the identity

$$\frac{1}{6}N(N+1)(N+2) = \frac{1}{2} \sum_{i=0}^N (N-2i)^2 = \sum_{i=0}^{N-1} (i+1)(N-i) \quad (\text{S19})$$

$$= \sum_{i=0}^N (N-2i)(N-i)(i+1) = - \sum_{i=0}^N (N-2i)(N-i+1)i, \quad (\text{S20})$$

we write  $C_2^0(N)$  using  $C_2^0(1)$ ,

$$C_2^0(N) = \frac{1}{6}N(N+1)(N+2)C_2^0(1) = \frac{1}{6}N(N+1)(N+2). \quad (\text{S21})$$

## LOCATION AND CHARGE OF YANG MONOPOLES FOR ODD $N$ AND POSITIVE $g$

Along the  $R_5$  axis, all off-diagonal couplings disappear and Fock states become the eigenstates. Varying  $R_5$ , we find  $N$  possible points on this axis where there exist four-fold degeneracy.

### (a) $N = 4m + 1$ for integer $m$

The four states,  $|m-l+1, m+l, m+l, m-l\rangle$ ,  $|m-l, m+l+1, m+l, m-l\rangle$ ,  $|m-l, m+l, m+l+1, m-l\rangle$ , and  $|m-l, m+l, m+l, m-l+1\rangle$  are degenerate at  $R_5 = -2lg$ , where  $l = -m, -m+1, \dots, m-1, m$ . The effective Hamiltonian reads

$$\tilde{\epsilon}_i = \epsilon_i \quad (\text{S22})$$

$$\tilde{t}_{ij} = t_{ij} \sqrt{(m-l+1)(m+l+1)}. \quad (\text{S23})$$

The extra Bose enhancement factor comparing to the single particle Hamiltonian does not change the second Chern number, so  $C_2 = 1$ .

At  $R_5 = -(2l+1)g$ , the other four states,  $|m-l-1, m+l+1, m+l+1, m-l\rangle$ ,  $|m-l, m+l, m+l+1, m-l\rangle$ ,  $|m-l, m+l+1, m+l, m-l\rangle$ , and  $|m-l-1, m+l+1, m+l+1, m-l\rangle$  are degenerate, where  $l = -m, -m+1, \dots, m-2, m-1$ . The effective Hamiltonian reads

$$\tilde{\epsilon}_i = -\epsilon_i \quad (\text{S24})$$

$$\tilde{t}_{ij} = t_{ij}^* \sqrt{(m-l)(m+l+1)}. \quad (\text{S25})$$

The extra Bose enhancement factor together with an additional phase factor  $e^{i\pi}$  comparing to the single particle Hamiltonian does not change the second Chern number but flipping the sign of the diagonal terms changes  $C_2$  to  $-1$ .

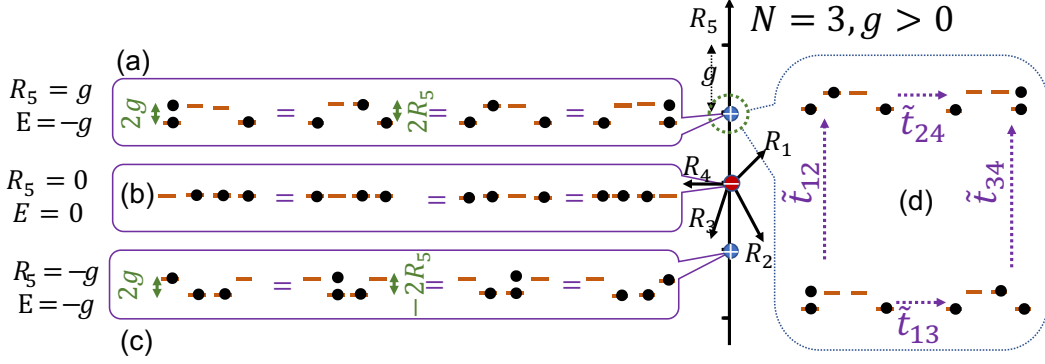


FIG. S1. (Color online) Schematic of Yang monopoles for 3 particles with positive interaction strength  $g$ . Blue (red) spheres show the positively (negatively) charged monopoles. Charges are denoted inside the sphere. The insets (a), (b), and (c) show the degenerate states at  $R_5 = g, 0,$  and  $-g,$  respectively; here  $R_1 = R_2 = R_3 = R_4 = 0$ . The inset (d) shows the effective Hamiltonian in the vicinity of  $R_5 = g, R_1 = R_2 = R_3 = R_4 = 0$ . Orange solid lines and black dots represent single particle states and bosons, respectively. Purple dotted arrows show effective couplings.

(b)  $N = 4m + 3$  for integer  $m$

At  $R_5 = -2lg$ , the four states,  $|m-l, m+l+1, m+l+1, m-l+1\rangle$ ,  $|m-l+1, m+l, m+l+1, m-l+1\rangle$ ,  $|m-l, m+l+1, m+l, m-l+1\rangle$ , and  $|m-l+1, m+l+1, m+l+1, m-l\rangle$  are degenerate, where  $l = -m, -m+1, \dots, m-1, m$ . The effective Hamiltonian reads

$$\tilde{\epsilon}_i = -\epsilon_i \quad (\text{S26})$$

$$\tilde{t}_{ij} = t_{ij}^* \sqrt{(m-l+1)(m+l+1)}. \quad (\text{S27})$$

Similar to case (a),  $C_2 = -1$ .

At  $R_5 = -(2l+1)g$ , the four states,  $|m-l+1, m+l+1, m+l+1, m-l\rangle$ ,  $|m-l, m+l+2, m+l+1, m-l\rangle$ ,  $|m-l, m+l+1, m+l+2, m-l\rangle$ , and  $|m-l, m+l+1, m+l+1, m-l+1\rangle$  are degenerate, where  $l = -m-1, -m, \dots, m-1, m$ . The effective Hamiltonian reads

$$\tilde{\epsilon}_i = \epsilon_i \quad (\text{S28})$$

$$\tilde{t}_{ij} = t_{ij} \sqrt{(m-l+1)(m+l+2)}. \quad (\text{S29})$$

Similar to case (a),  $C_2 = 1$ .

For example, Fig. S1(d) illustrates the effective Hamiltonian for  $N = 3$  and  $R_5 = g$ . The onsite energy different balances off the repulsive energy for the sites with two particles. Thus, all the four states has the same energy and as the coupling  $R_1, R_2, R_3, R_4$  approaches zero, the four states becomes the eigenstates and four-fold degeneracy emerges.

## $C_2$ FOR ODD $N$

The second Chern number on any closed 4D surface is equal to the total charge of monopoles inside the surface. For example, we choose the surface of a 5D sphere centered at the origin and calculate the Chern number. The solid and dashed lines in Fig. S2 show the Chern number for 3 particles as a function of the radius of the sphere for positive and negative  $g$ , respectively. For repulsive interaction, as the radius increases, the integration sphere encloses more and more monopoles and the second Chern number alternates between 1 and  $-1$  and becomes 1 for large interaction sphere. At each transition point, the change of  $C_2$  is 2 ( $-2$ ) because the integration sphere touches a pair of positively (negatively) charged monopoles. For attractive interaction, the second Chern number is a constant because a integration sphere that centered at the origin always enclose the monopole.

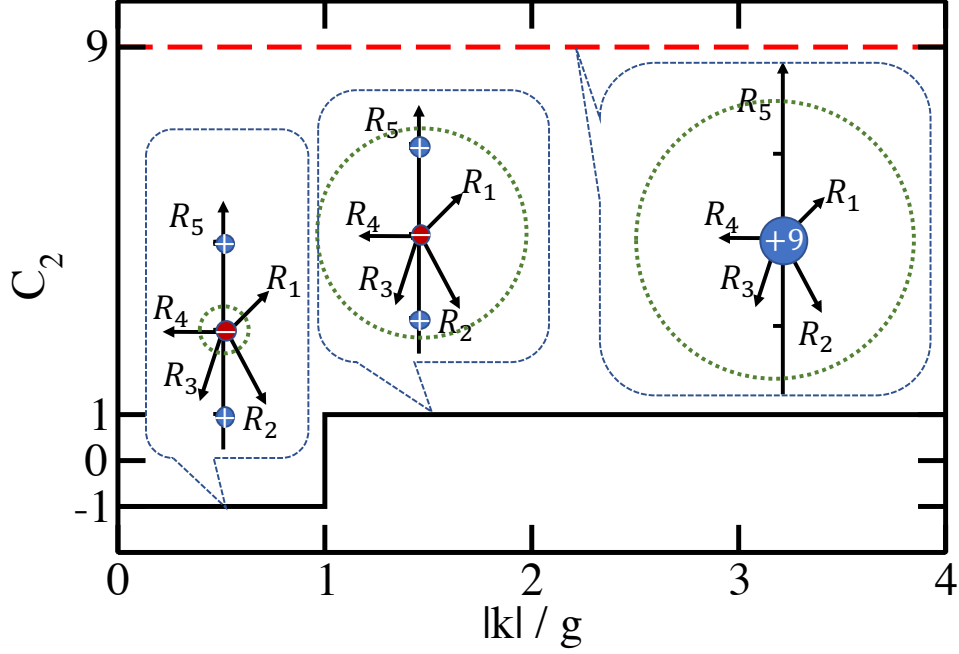


FIG. S2. (Color online) Second Chern number as a function of the radius  $|k|$  of the 5D sphere. The solid and dashed lines are for systems with repulsive and attractive interactions, respectively. The insets illustrate the distribution of monopole at three different points of the graph. The green dotted lines show the surface schematically.

### EXPRESSION FOR $c_N$

At the origin,  $|N, 0, 0, 0\rangle$ ,  $|0, N, 0, 0\rangle$ ,  $|0, 0, N, 0\rangle$ ,  $|0, 0, 0, N\rangle$  are the four degenerate many-body ground states. Treating the  $|R|$  as a small parameter, the lowest order coupling reads

$$\langle N, 0, 0, 0 | \hat{H}_{\text{eff}} | 0, N, 0, 0 \rangle = \frac{\prod_{i=0}^{N-1} \langle N-i, i, 0, 0 | \hat{K} | N-i-1, i+1, 0, 0 \rangle}{\prod_{i=1}^{N-1} \left( \langle N-i, i, 0, 0 | \hat{U} | N-i, i, 0, 0 \rangle - \langle N, 0, 0, 0 | \hat{U} | N, 0, 0, 0 \rangle \right)}. \quad (\text{S30})$$

Other terms can be written similarly. Comparing with the expression in the main text, we have

$$c_N = \frac{\prod_{i=0}^{N-1} \sqrt{(N-i)(i+1)}}{\prod_{i=1}^{N-1} [(N-i)^2 + i^2 - N^2]}. \quad (\text{S31})$$

### 3D TOPOLOGICAL DEFECTS FOR EVEN NUMBER OF PARTICLES WITH REPULSIVE INTERACTION

For later convenience, we introduce  $R_A$ ,  $R_B$ ,  $\phi_A$ , and  $\phi_B$ , which are defined through  $R_A e^{-i\phi_A} = R_x - iR_y$  and  $R_B e^{-i\phi_B} = R_z n_x - iR_z n_y$ . For  $4m$  particles with strong repulsive interaction, the ground state is  $|m, m, m, m\rangle$ . No degeneracy is found.

For  $4m+2$  particles with strong repulsive interaction, the ground state manifold has 6 states,  $|m, m, m+1, m+1\rangle$ ,  $|m, m+1, m, m+1\rangle$ ,  $|m, m+1, m+1, m\rangle$ ,  $|m+1, m, m, m+1\rangle$ ,  $|m+1, m, m+1, m\rangle$ , and  $|m+1, m+1, m, m\rangle$ . The Hamiltonian reads

$$\begin{pmatrix} 0 & 0 & -e^{i\phi_B}(m+1)R_B & -e^{i\phi_B}(m+1)R_B & 0 & 0 \\ 0 & 0 & e^{i\phi_A}(m+1)R_A & -e^{i\phi_A}(m+1)R_A & 0 & 0 \\ -e^{-i\phi_B}(m+1)R_B & e^{-i\phi_A}(m+1)R_A & 2R_5 & 0 & -e^{i\phi_A}(m+1)R_A & -e^{i\phi_B}(m+1)R_B \\ -e^{-i\phi_B}(m+1)R_B & -e^{-i\phi_A}(m+1)R_A & 0 & -2R_5 & e^{i\phi_A}(m+1)R_A & -e^{i\phi_B}(m+1)R_B \\ 0 & 0 & -e^{-i\phi_A}(m+1)R_A & e^{-i\phi_A}(m+1)R_A & 0 & 0 \\ 0 & 0 & -e^{-i\phi_B}(m+1)R_B & -e^{-i\phi_B}(m+1)R_B & 0 & 0 \end{pmatrix} \quad (\text{S32})$$

Two of the states, i.e.  $(|0, 0, 1, 1\rangle - e^{-2i\phi_B} |1, 1, 0, 0\rangle)/\sqrt{2}$  and  $(|0, 1, 0, 1\rangle + e^{-2i\phi_A} |1, 0, 1, 0\rangle)/\sqrt{2}$ , have zero energy. Projecting out these two states, we write the effective Hamiltonian as a 4 by 4 matrix,

$$\begin{pmatrix} 2R_5 & \sqrt{2}e^{-i\phi_A}(m+1)R_A & -\sqrt{2}e^{-i\phi_B}(m+1)R_B & 0 \\ \sqrt{2}e^{i\phi_A}(m+1)R_A & 0 & 0 & -\sqrt{2}e^{i\phi_A}(m+1)R_A \\ -\sqrt{2}e^{i\phi_B}(m+1)R_B & 0 & 0 & -\sqrt{2}e^{i\phi_B}(m+1)R_B \\ 0 & -\sqrt{2}e^{-i\phi_A}(m+1)R_A & -\sqrt{2}e^{-i\phi_B}(m+1)R_B & -2R_5 \end{pmatrix}. \quad (\text{S33})$$

Rewriting the effective Hamiltonian using direct product of  $\sigma$  and  $\tau$  matrices, we obtain

$$R_5(\tau_z + \sigma_z) + (R'_1\sigma_x + R'_2\sigma_y - R'_3\tau_x + R'_4\tau_y + \tau_z(R'_3\tau_x + R'_4\tau_y) + \tau_z(R'_1\tau_x - R'_2\tau_y)), \quad (\text{S34})$$

where  $R'_1 = (m+1)(R_1 - R_3)/\sqrt{2}$ ,  $R'_2 = (m+1)(R_2 + R_4)/\sqrt{2}$  and  $R'_3 = (m+1)(R_1 + R_3)/\sqrt{2}$ , and  $R'_4 = (m+1)(R_2 - R_4)/\sqrt{2}$ . Solving the effective Hamiltonian, the eigen energies reads

$$\pm \sqrt{2}(m+1) \sqrt{\pm \sqrt{\left( (R_A^2 + R_B^2) + \frac{R_5^2}{(m+1)^2} \right)^2 - 4R_A^2 R_B^2 + R_A^2 + R_B^2 + \frac{R_5^2}{(m+1)^2}}}. \quad (\text{S35})$$

Eigenenergies become degenerate in certain 3D continuous manifolds.

$\{\mathcal{M}_1: R_A = 0\}$  and  $\{\mathcal{M}'_1: R_B = 0\}$ , the second and the third states are degenerate, and the ground state (the fourth state) is unique.

$\{\mathcal{M}_2: R_5 = 0, R_A = R_B\}$ , both the ground and excited states are doubly degenerate.

For  $M_1$  and  $M'_1$ , we find that the berry phase  $\gamma = (0, 2\pi, 2\pi, 0)$  and  $\zeta_1 = 0$  for the lowest two states. For  $M_2$ , we find that  $\gamma = \pi$  for all eigenstates and  $\zeta_1 = 0$  for the lowest two states.

We also rewrite the manifolds in the main text using  $R_A$  and  $R_B$  and find that the two type of 3D manifolds are switched with each other as the interaction strength changes from negative to positive. Furthermore, we have numerically verified that these degenerate manifolds extend to the weakly interacting regime.

## LINKING NUMBER

In the 3D subspace with finite  $|\vec{m}|$ , e.g.,  $R_3 \neq 0$  and  $R_4 = 0$ ,  $\mathcal{M}_1$  and  $\mathcal{M}_2$  are knotted nodal line and nodal ring. Thus, a linking number can be defined as follows,

$$L = \frac{1}{4\pi} \oint_{\mathcal{M}_1} \oint_{\mathcal{M}_2} \frac{\mathbf{r}_1 - \mathbf{r}_2}{|\mathbf{r}_1 - \mathbf{r}_2|^{\frac{3}{2}}} \cdot d\mathbf{r}_1 \times d\mathbf{r}_2. \quad (\text{S36})$$

A straightforward calculation shows that  $L$  is always 1, which verifies that the two nodal surfaces are knotted in the subspace.